Environmental Science & Technology

pubs.acs.org/est

Article

Comparison of Simultaneous Measurements of Indoor Nitrous Acid: Implications for the Spatial Distribution of Indoor HONO Emissions

Brandon Bottorff,* Chen Wang, Emily Reidy, Colleen Rosales, Delphine K. Farmer, Marina E. Vance, Jonathan P. D. Abbatt, and Philip S. Stevens

Cite This: *Environ. Sci. Technol.* 2022, 56, 13573−13583

Read Online

ACCESS | Metrics & More | Article Recommendations

ABSTRACT: Despite its importance as a radical precursor and a hazardous pollutant, the chemistry of nitrous acid (HONO) in the indoor environment is not fully understood. We present results from a comparison of HONO measurements from a time-of-flight chemical ionization mass spectrometer (ToF-CIMS) and a laser photofragmentation/laser-induced fluorescence (LP/LIF) instrument during the House Observations of Microbial and Environmental Chemistry (HOMEChem) campaign. Experiments during HOMEChem simulated typical household activities and provided a dynamic range of HONO mixing ratios. The instruments measured HONO at different locations in a house featuring a typical air change rate (ACR) (0.5 h^{-1}) and an enhanced mixing rate (~8 h^{-1}). Despite the distance between the instruments, measurements from the two instruments agreed to within their respective uncertainties (slope = 0.85, R^2 = 0.92), indicating that the lifetime of HONO is long enough for it to be quickly distributed indoors, although spatial gradients occurred during ventilation periods. This suggests that emissions of HONO from any source can mix throughout the house and can contribute to OH radical production in sunlit regions, enhancing the oxidative capacity indoors. Measurement discrepancies were likely due to interferences with the LP/LIF instrument as well as calibration uncertainties associated with both instruments.

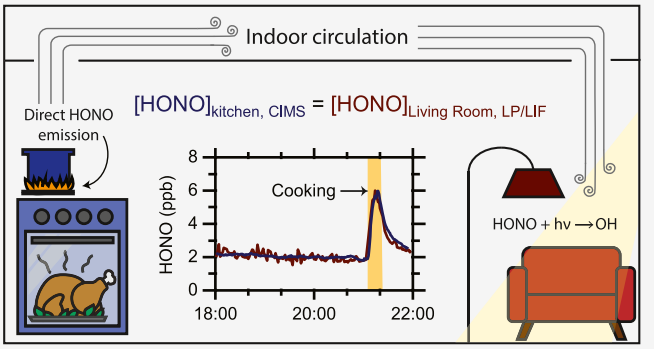

KEYWORDS: *indoor air pollution, radical production, indoor emissions, photolysis, ventilation, indoor air chemistry*

INTRODUCTION

Nitrous acid (HONO) plays an important role in the chemistry of the atmosphere. Photolysis of HONO can lead to the production of hydroxyl radicals (OH), the dominant oxidant in the outdoor atmosphere (R1). In the presence of NO_x, reactions of OH with volatile organic compounds (VOCs) establish a fast radical propagation cycle that can produce harmful secondary pollutants. While ozone photolysis can be a significant source of OH throughout the day,[1,2] several studies have suggested that the photolysis of HONO (R1) can be a significant and often dominant source of OH in the outdoor atmosphere, contributing up to 40% of total radical production in several summer studies[3−6] and more than 80% in some winter campaigns.[7−9] As such, understanding HONO chemistry is essential to characterizing the overall oxidative capacity of the atmosphere.

$$\mathrm{HONO} + h\nu\ (300\ \mathrm{nm} < \lambda < 400\ \mathrm{nm}) \rightarrow \mathrm{OH} + \mathrm{NO} \quad \text{(R1)}$$

HONO is also an important indoor pollutant, with mixing ratios that are often much higher than outdoors. Lee et al. measured outdoor HONO mixing ratios of 0.9 ppb compared to 4.6 ppb within nearby buildings,[10] and Leaderer et al. measured HONO mixing ratios of 0.3 ppb outdoors compared to 4.0 ppb within residences that utilized gas stoves.[11] Furthermore, other measurements have shown that indoor HONO mixing ratios can reach 20−90 ppb during cooking or other combustion events.[12−15] While combustion within the indoor environment is a primary source of HONO, recent studies have shown that abundant interior surfaces provide an important reservoir for HONO.[16−18] Several studies have shown that elevated HONO mixing ratios could result in OH radical concentrations comparable to those found outdoors, despite attenuation from glass windows resulting in reduced photolysis frequencies that limit OH production by primary photolytic processes.[12,19−21]

Received: March 29, 2022
Revised: August 24, 2022
Accepted: August 26, 2022
Published: September 22, 2022

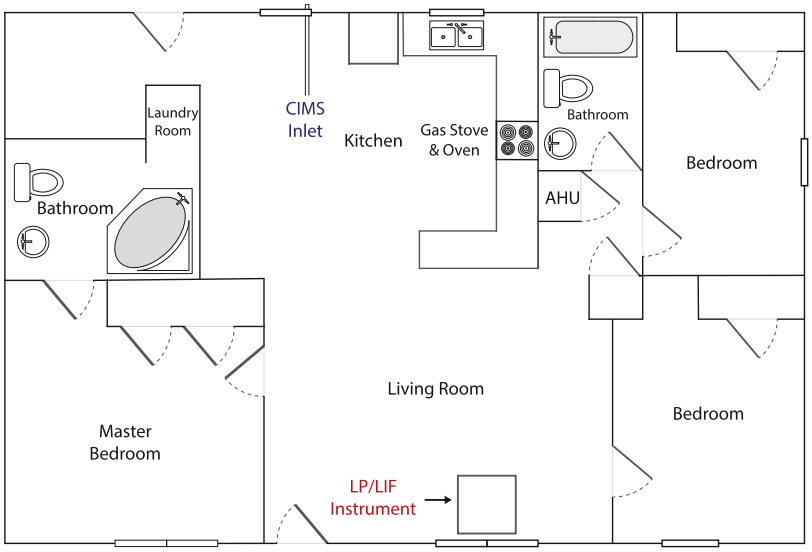

Figure 1. Floorplan of the UTest house with the CIMS (blue) and LP/LIF (red) sampling locations highlighted.

Despite its importance as an indoor health hazard and a precursor to radical concentrations, the emissions and chemistry of indoor HONO are still not fully understood, in part due to the challenge associated with accurate measurements of HONO.[22] Sampling artifacts from the heterogeneous formation of HONO inside inlet lines or on surfaces are a common concern for many instruments, and interferences from other species such as NO_2 and peroxyacetyl nitrate (PAN) must be considered.[23,24] Current instruments use a variety of techniques, including reducing residence times and minimizing surfaces to reduce inlet artifacts, and the use of secondary channels to quantify interferences.[22,24,25]

There have been several recent intercomparisons of HONO measurements in outdoor settings.[23,26−29] Discrepancies between the measurements have been attributed to interfering species, saturation effects of some instruments at higher concentrations, or spatial heterogeneity due to nearby HONO sources and distance between inlets.[27−29] During the Study of Houston Atmospheric Radical Precursors (SHARP) campaign, which involved six different HONO instruments, Pinto et al.[28] noted that the agreement between instruments with co-located inlets was better than that for instruments that were spatially separated by several meters, suggesting that various sources of HONO could cause spatial differences in outdoor HONO concentrations.

In contrast, there have been no previous intercomparisons of HONO measurements in residential environments. Indoor instrumental intercomparisons not only provide a test of advanced measurement techniques but can also provide important information on the spatial and temporal distribution of indoor emissions, especially reactive emissions such as HONO. A recent computational fluid dynamics (CFD) study suggested that HONO concentrations from a combustion source would be relatively evenly distributed in a representative indoor setting, but OH and HO_2 radical production from HONO photolysis would be confined to sunlit areas.[30] On the other hand, it has been shown that HONO formation through heterogeneous reactions of surface NO_2 can be enhanced in sunlit regions of the indoor environment.[31−33] Measurements of the production of HONO from light-induced heterogeneous reactions of NO_2 with grime adsorbed on glass windows suggest that indoor HONO concentrations may be greater in sunlight kitchen areas compared to other indoor areas.[34]

Given the importance of HONO to OH radical production, measurements of the spatial distribution of HONO emissions indoors are needed to fully understand the oxidative capacity of indoor environments. In this paper, we describe HONO measurements from within a house by two different instruments that sampled indoor air at two different locations: a laser photofragmentation/laser-induced fluorescence (LP/LIF) instrument and a time-of-flight chemical ionization mass spectrometer (ToF-CIMS). The measurements were conducted as part of the House Observations of Microbial and Environmental Chemistry (HOMEChem) study, during which a variety of cooking, cleaning, occupation, and ventilation experiments resulted in a dynamic range of HONO mixing ratios. The measurements also provided information on the spatial distribution and lifetime of HONO concentrations in a typical indoor environment. While Wang et al.[18] presented a detailed discussion of processes affecting HONO mixing ratios during HOMEChem, this paper focuses on the first intercomparison between simultaneous measurements from two different locations in a house, and the associated implications for spatial gradients of HONO in indoor spaces.

EXPERIMENTAL METHODS

HOMEChem Study. The HOMEChem study was a large-scale collaborative field study designed to investigate the chemical transformations within a residential environment during a variety of realistic household events.[35] HOMEChem took place in June 2018 at the UTest House within the J.J. Pickle Research Campus of the University of Texas at Austin (Figure 1). The house is a 111 m^2, three-bedroom, two-bathroom manufactured home with two separate heating ventilation and air-conditioning (HVAC) systems with underfloor and overhead air diffusers. However, only the overhead system was utilized to provide more rapid mixing during air-conditioning. During the campaign, the fan in the HVAC system operated continuously and moved air at a rate of 2000 m^3/h (approximately 8 house volumes per hour) to provide consistent mixing in the house throughout the campaign. A separate system also delivered a constant flow of outdoor air,

https://doi.org/10.1021/acs.est.2c02196
Environ. Sci. Technol. 2022, 56, 13573−13583

which provided an average air change rate (ACR) of 0.5 ± 0.1 h^{-1} when the doors and windows were closed. The house thermostat was typically set at 25 °C during the campaign, with exceptions made for some experiments.

Experiments were separated into several day-long categories with a focus on sequential experiments, layered experiments, and Thanksgiving simulations. Sequential experiments consisted of several cooking, cleaning, occupancy, or ventilation events throughout the day and were designed to provide repeatable tests to examine the emissions and chemical processes following isolated activities. After sequential cooking, cleaning, and occupancy events, a period of time was allowed to observe chemical activity, and then the doors and windows of the house were opened to provide enhanced ventilation prior to the next repetition of the experiment. Layered days consisted of multiple occupants performing both cooking and cleaning events on the same day without ventilation periods. Layered days were designed to simulate a typical day in a residential setting and to examine the combined effects of different types of emissions over an extended period. Thanksgiving experiments consisted of prolonged cooking periods and several occupants to simulate a typical North American holiday setting. All of the measurements and experiments performed during HOMEChem, along with a complete description of test house conditions, are described elsewhere.[35]

Laser Photofragmentation/Laser-Induced Fluorescence Instrument. The laser photofragmentation/laser-induced fluorescence (LP/LIF) instrument has been described in detail elsewhere,[36] thus only a brief description will be given here. The LP/LIF technique detects HONO after expansion of ambient air into a low-pressure cell by photolysis into OH and NO fragments via a 355 nm laser emission, and subsequent detection of the OH fragment by laser-induced fluorescence at 308 nm. The photofragmentation laser system consists of Spectra Physics Navigator II YHP40-355 HM neodymium-doped yttrium aluminum garnet (Nd:YAG) laser that produces approximately 3−4 W of radiation at 355 nm at a repetition rate of 10 kHz, and the excitation laser system consists of a Spectra Physics Navigator YHP40-532 Nd:YAG laser that produces 7−8 W of radiation at 532 nm. This laser pumps a Sirah Credo dye laser to produce approximately 40−100 mW of radiation at 308 nm. During HOMEChem, both laser systems were housed in a trailer adjacent to the test house and laser emissions were propagated to the sampling cell by 12 m fiber optic cables, and the low-pressure sampling cell was placed in the UTest house living room near the western-facing glass windows (Figure 1). These windows received direct sunlight on most days between 17:00 and 19:00 local time.

Ambient air is drawn into the low-pressure sampling cell through a flat 1 mm diameter pinhole inlet and expanded into the sampling cell. The cell is maintained at a pressure of approximately 0.25 kPa to reduce quenching of the OH fluorescence by ambient air and thus increase the OH radical fluorescence lifetime. Sampling through the flat inlet into the low-pressure cell also effectively minimizes the potential for inlet artifacts caused by the formation of HONO on inlet lines or instrument surfaces. After exiting their respective fiber optic cables, the 355 and 308 nm laser emissions are spatially joined by a dichroic mirror before entering the detection cell. The laser pulses are temporally separated, with the 308 nm pulse entering the detection cell 100 ns after the 355 nm pulse. Fluorescence from the OH radical fragment is collected at right angles to both the sampled air stream and the laser emissions and detected using a micro-channel plate (MCP) photomultiplier tube (Photek PMT325) and a time-gated detection scheme.[36]

To distinguish ambient OH fluorescence from background signals, wavelength modulation is used to tune the 308 nm dye laser emission on- and off-resonance with the $Q_1(3)$ transition of OH at 308.1451 nm. The net signal from OH fluorescence is derived by subtracting the on-resonance signal from the background, which is composed primarily of scattered laser radiation that extends into the detection window. To differentiate OH fluorescence signals due to HONO photofragmentation from those due to ambient OH radicals, the 355 nm fragmentation laser is cycled on and off with the use of a shutter.

The LP/LIF instrument calibration consists of two stages. First, the instrumental sensitivity to OH (R_{OH}) is determined via the ultraviolet (UV) photolysis of water vapor at 185 nm that has been described in detail previously.[37] This calibration was conducted before, during, and after the HOMEChem campaign. With a known sensitivity toward OH, measurements of the photolysis efficiency (PE) of the 355 nm laser allow the determination of the instrumental sensitivity toward HONO.[36] A known amount of OH and HO_2 is produced within the calibration source and an excess of NO is added to convert OH and HO_2 in the calibrator to HONO. When the 355 nm photolysis laser is turned on, a portion of HONO is converted back to OH in the sampling cell. The photolysis efficiency is defined as the ratio of OH signal from photo-fragmented HONO to the sum of OH and HO_2 produced by the calibrator. While typical PE calibrations introduce a maximum of 2 ppb of HONO into the detection cell, the MCP detector response during direct OH calibrations remains linear at OH mixing ratios as high as 1 ppb. Only a small fraction (0.34%) of HONO is photolyzed by the 355 nm laser, suggesting a linear response to HONO mixing ratios of at least 300 ppb. Photolysis efficiency calibrations were conducted before and after the campaign to avoid adding NO from the calibration procedure into the house. During the campaign, 355 and 308 nm laser powers within the sampling cell averaged 1.4 W and 3.0 mW respectively. This resulted in an instrumental sensitivity to OH of approximately 2.75 × 10^{-8} counts/s/cm^3/mW and a measured photolysis efficiency of 0.34%. The limit of detection for HONO was approximately 9 ppt (S/N = 1, 10 min average) based on the standard deviation of the background signal.[36,38] The overall calibration uncertainty during HOMEChem was approximately ±35% primarily due to the precision of the measurement of the photofragmentation efficiency (±25%). As discussed below, the precision of the measurement varied between approximately 20 and 30% during the campaign due to variations in laser power, alignment, and wavelength that impacted the on-line signal.

Chemical Ionization Mass Spectrometry Instrument. The chemical ionization mass spectrometry (CIMS) instrument was operated from a second trailer adjacent to the test house. Instrumental details including potential interferences and the specific setup at HOMEChem have been described elsewhere.[16−18] Briefly, the CIMS instrument utilized acetate as the reagent ion and detected HONO as NO_2^- in the mass spectrometer at m/z 45.9. The mass resolving power ($M/\Delta M$) was approximately 4000 during the campaign. Sampling occurred in the kitchen of the house (Figure 1), approximately 5 m away from the LP/LIF sampling cell, through a 10 m

https://doi.org/10.1021/acs.est.2c02196
Environ. Sci. Technol. 2022, 56, 13573−13583

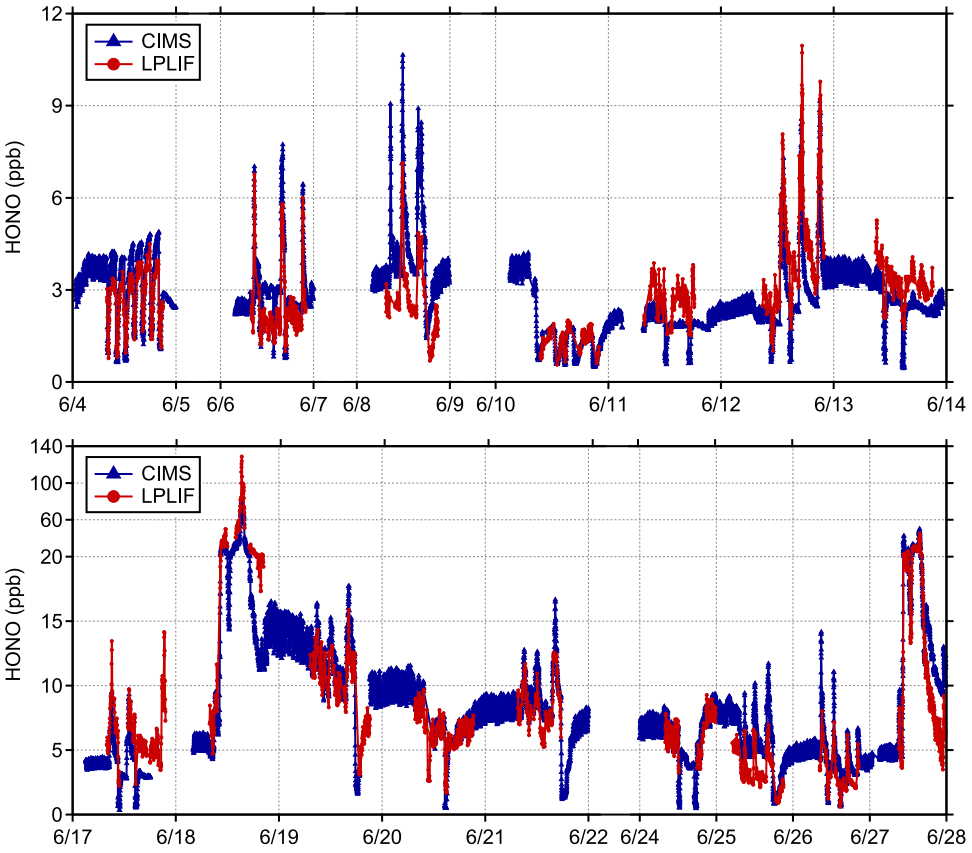

Figure 2. Time series of all HONO measurements during HOMEChem by the CIMS instrument (blue) and the LP/LIF instrument (red).

perfluoroalkoxy (PFA) tube at a flow rate of 2.1 L/min. During the campaign, the potential for HONO formation in the 10 m inlet tube was investigated by passing indoor air through an annular denuder containing Na_2CO_3. With the denuder scrubbing ambient HONO prior to the 10 m tube, the nitrite ion signal was reduced to <10% of its initial value, suggesting that at least 90% of the signal is due to HONO. A three-way solenoid isolation valve allowed switching between the kitchen inlet, a zero-air background, and an outdoor inlet for 53, 2, and 5 min of each hour, respectively. The kitchen area received direct sunlight on most days between approximately 9:00 and 12:00 local time through the eastern-facing windows.

The CIMS instrument was calibrated before and after the campaign using a HONO source with an output from 1 to 10 ppb.[16,18] A secondary calibration was also performed on-site each day in which ambient gaseous HONO was collected in deionized water followed by aqueous nitrite analysis using an ultraviolet−visible (UV−vis) spectrophotometric technique.[16] A linear relationship between the CIMS signal and HONO from this daily calibration was observed. An averaged sensitivity factor from the primary calibration method was used for measurements made at the beginning and end of the campaign, but a sensitivity change required the on-site calibration technique to be used from June 5 to 17. Furthermore, as previous studies have shown that CIMS sensitivity can decrease with increasing humidity, additional calibrations were conducted after the campaign that revealed only a 10% decrease in sensitivity when relative humidity (RH) was increased from 10 to 60%. This weak sensitivity dependence on humidity is similar to that observed by another CIMS instrument that also utilized acetate as the reagent ion.[39] As the RH measured inside the house typically varied between 40 and 60% over the course of the campaign, humidity is not expected to be an important factor in the acetate-CIMS sensitivity to HONO.

High total ion signals during intense cooking activities reduced reagent ion signals and required dilution of indoor air on some days. During these periods, a flow of high-purity nitrogen was added prior to the CIMS inlet. Data presented below have been corrected for dilution periods but may be subject to a higher uncertainty than nondilution periods. Uncertainty of the reported HONO mixing ratios is estimated to be approximately ±30%. The limit of detection (3σ) of HONO for the CIMS was determined from the standard deviation during background (zero air) measurements of the 1 s data and is lower than 50 ppt. The calculated precision of the CIMS when measuring 2.5 ppb of HONO from a custom-built HONO source was approximately 50 ppt.

RESULTS

General Behavior. A comprehensive time series of all measurements from the HOMEChem campaign that are considered in the intercomparison is shown in Figure 2. As described in Farmer et al.,[35] a variety of unique experiments were performed over the course of the campaign to analyze the effect of household activities on trace-gas mixing ratios, particle formation and composition, and surface chemistry. As gas-phase HONO mixing ratios were most significantly influenced by cooking, bleach cleaning, and ventilation experiments, these experiments were chosen as case studies and the measurement agreement and behavior during these periods is discussed in more detail below. Measured HONO mixing ratios during

https://doi.org/10.1021/acs.est.2c02196
Environ. Sci. Technol. 2022, 56, 13573−13583

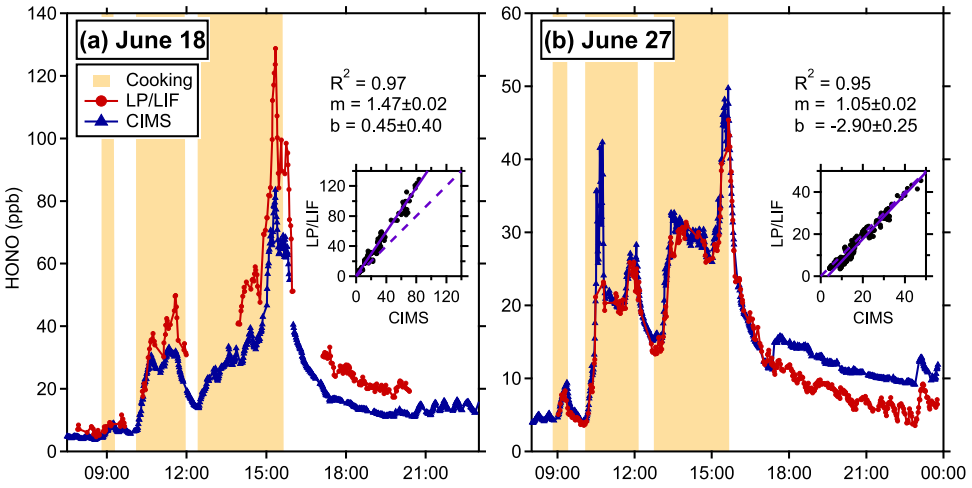

Figure 3. CIMS (blue) and LP/LIF (red) measurements of HONO from Thanksgiving experiments on (a) June 18 and (b) June 27. Shaded regions indicate active propane-cooking periods. A bivariate weighted fit of the data is also shown with the regression slope (m) and y-intercept (b) (see text).

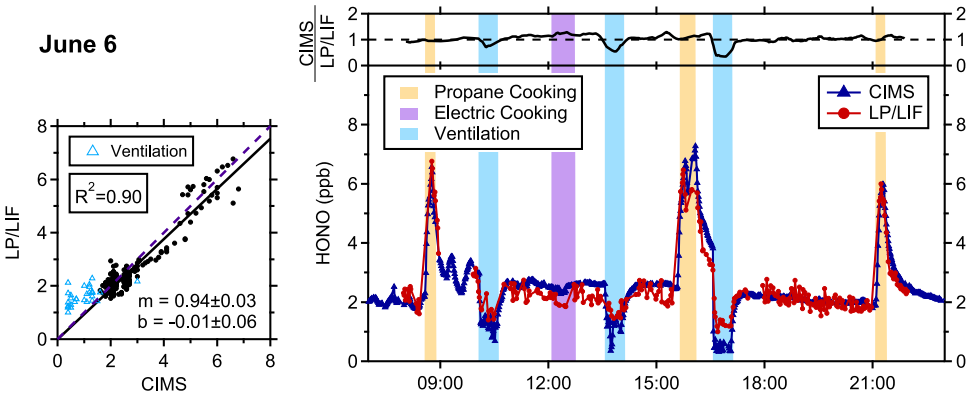

Figure 4. CIMS (blue) and LP/LIF (red) as well as the ratio of the CIMS and LP/LIF measurements of HONO from a sequential cooking experiment on June 6. Shaded areas indicate ventilation (blue) and active propane (orange) and electric hotplate (purple) cooking experiments. Measurements during ventilation periods are not included in the correlation (see text).

these experiments ranged from as low as 0.2 ppb during a ventilation period to over 100 ppb during a Thanksgiving cooking experiment. Other factors, including air conditioner operation, vinegar cleaning, and ozone addition also influenced HONO concentrations. For a more comprehensive analysis and discussion of HONO behavior during these experiments, see Wang et al.[18]

Cooking Experiments. Emissions during propane gas cooking, both direct emissions of HONO and emissions of NO_x followed by the subsequent reaction on surfaces, led to the highest observed mixing ratios of HONO throughout the campaign. Figure 3 illustrates the measurements during the two simulated Thanksgiving experiments. On these days (June 18 and 27), four volunteers prepared a large meal representative of a North American holiday gathering. The gas oven and stove were used continuously between approximately 9:00 and 15:00 (shaded periods in Figure 3) with breaks for breakfast and lunch. Following the cooking period, approximately 15 occupants entered the house for 1.5 h. As multiple stovetop burners were operated continuously during the 6−7 h cooking experiment, Thanksgiving Day simulations can ultimately be described as long duration and high-intensity gas-cooking experiments followed by a high-occupancy period.

During the June 18 Thanksgiving experiment, LP/LIF and CIMS measurements reached the maximum values observed during the campaign of 128 and 84 ppb, respectively. Decreases in gas-phase HONO mixing ratios after cooking were faster than the expected loss due to air exchange alone, likely due to dilution into the rest of the house followed by dilution from air exchange and deposition to interior surfaces. Prior to the cooking emissions on this day, background HONO mixing ratios in the absence of perturbations were approximately 3 ppb (Figure 2, June 4−17). After the cooking events on June 18, background HONO mixing ratios remained above 5 ppb for several days (Figure 2, June 19−24). These elevated background levels of HONO are likely due to an enhancement of the surface HONO reservoir following the intense cooking activities on June 18. During the June 27 Thanksgiving experiment, both instruments observed maximum values of approximately 50 ppb.

The measured mixing ratios of HONO by both instruments were highly correlated, with R^2 values of at least 0.95 on each day (Figure 3). However, the LP/LIF measurements during the June 18 Thanksgiving experiment were on average 47% higher than the CIMS measurements throughout the day. The reason for this discrepancy is unclear but may be related to uncertainties in the sensitivity of the CIMS instrument during

https://doi.org/10.1021/acs.est.2c02196
Environ. Sci. Technol. 2022, 56, 13573−13583

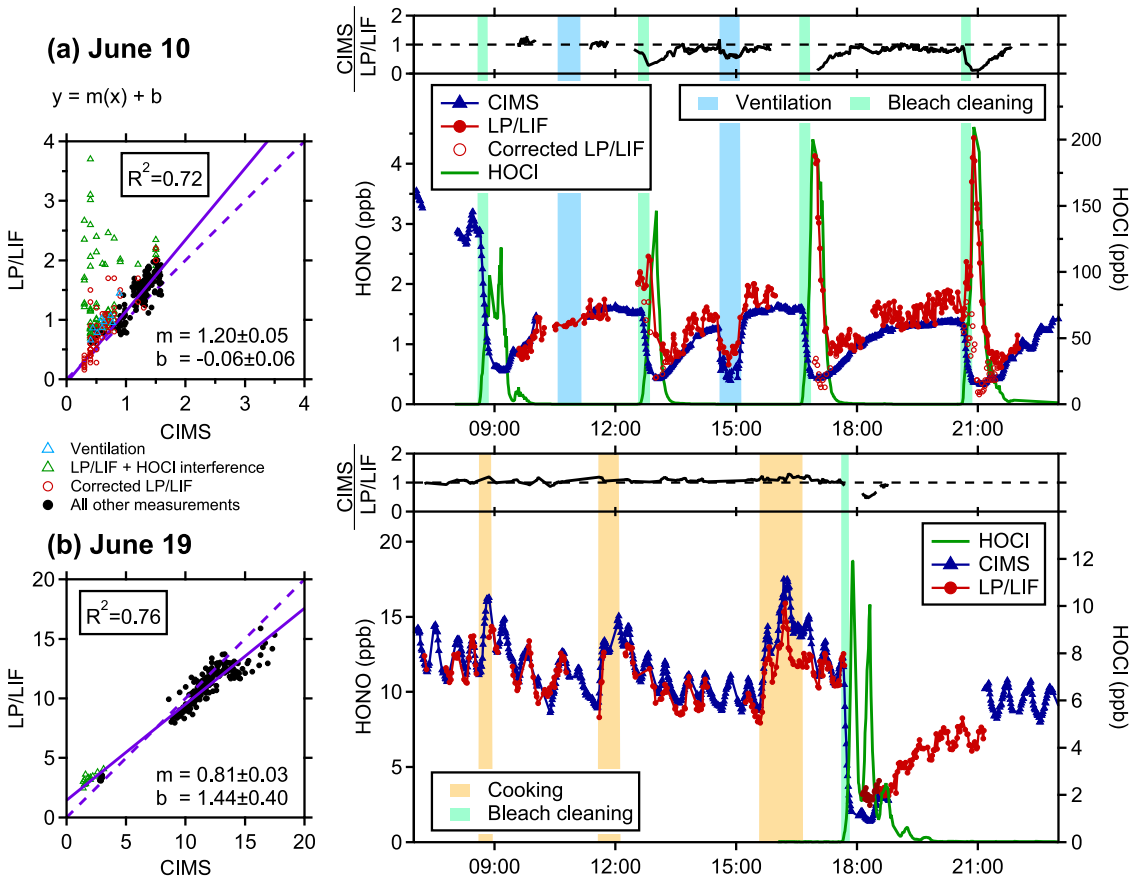

Figure 5. CIMS (blue) and LP/LIF (red) measurements of HONO as well as the ratio of the CIMS and LP/LIF measurements, and HOCl measurements from a time-of-flight chemical ionization mass spectrometer (ToF-CIMS) paired with iodide (I^-) chemical ionization (green) from (a) sequential bleach cleaning experiments (June 10) and (b) a layered experiment (June 19). Blue-, green-, and orange-shaded regions represent ventilation, bleach cleaning, and cooking periods, respectively. Measurements when HOCl was high (green triangles), measurements during ventilation periods (blue triangles), and LP/LIF measurements corrected for the HOCl interference (open red circles) are not included in the correlation analysis (see text).

the use of the dilution flow on this day. Another possibility for the discrepancy is that changes in the alignment of the photofragmentation laser over the course of the campaign led to a change in the photofragmentation efficiency of the LP/LIF instrument that was greatest on this day. In contrast, the measurements during the June 27 experiment were in excellent agreement during most of the day, with a bivariate least-squares fit of the data weighted by the precision of both measurements to account for the uncertainty associated with each, resulting in a slope of 1.05 ± 0.02 and intercept that is relatively small compared to the measured HONO mixing ratios. On this day, the CIMS measurements agreed with the LP/LIF measurements until approximately 17:00 when the dilution flow was stopped, resulting in the CIMS measurements appearing to be systematically greater than the LP/LIF measurements. The reason for this discrepancy is not known but may be due to an unidentified error associated with the dilution flow impacting the sensitivity or ion chemistry of the instrument for this period only.

Figure 4 shows measurements of HONO during a sequential cooking experiment. In contrast to the Thanksgiving experiments, sequential cooking experiments and cooking events performed on layered days typically utilized a single propane stove burner and were performed on a shorter timescale (orange-shaded periods in Figure 4). On average, these repeated cooking experiments typically enhanced HONO mixing ratios by approximately 5 ppb above the background levels, whereas control experiments, in which the same cooking procedure was carried out on an electric hotplate (purple-shaded region in Figure 4), did not emit HONO. Similar to the Thanksgiving experiments, the HONO measurements by the two instruments were in excellent agreement, with a weighted fit of the data on the June 6 sequential cooking experiment resulting in a correlation plot with a slope of 0.94 ± 0.03 and an R^2 value of 0.90 (Figure 4), with y-intercepts that are very small compared to the measured mixing ratios.

Bleach Cleaning Experiments. Bleach cleaning experiments were performed on June 10, a sequential cleaning day, and at the conclusion of each layered day experiment (June 8, 19, 21, and 25). For each bleach cleaning experiment, one volunteer prepared a bleach solution (120 mL of a commercial sodium hypochlorite solution in 2.3 L of tap water) according to manufacturer instructions before applying the solution to the floors of the house with a sponge mop for 10 min. The measurements of HONO during the June 10 sequential bleach cleaning and the June 19 layered experiment are shown in Figure 5. As described in Wang et al.,[18] gas-phase HONO mixing ratios typically dropped quickly after each bleach episode. This is likely due to the dissolution of gas-phase HONO into the basic bleach solution followed by the reaction of nitrite on surfaces with reactive chlorinated species deposited within the bleach solution,[40] such as the reaction

https://doi.org/10.1021/acs.est.2c02196
Environ. Sci. Technol. 2022, 56, 13573−13583

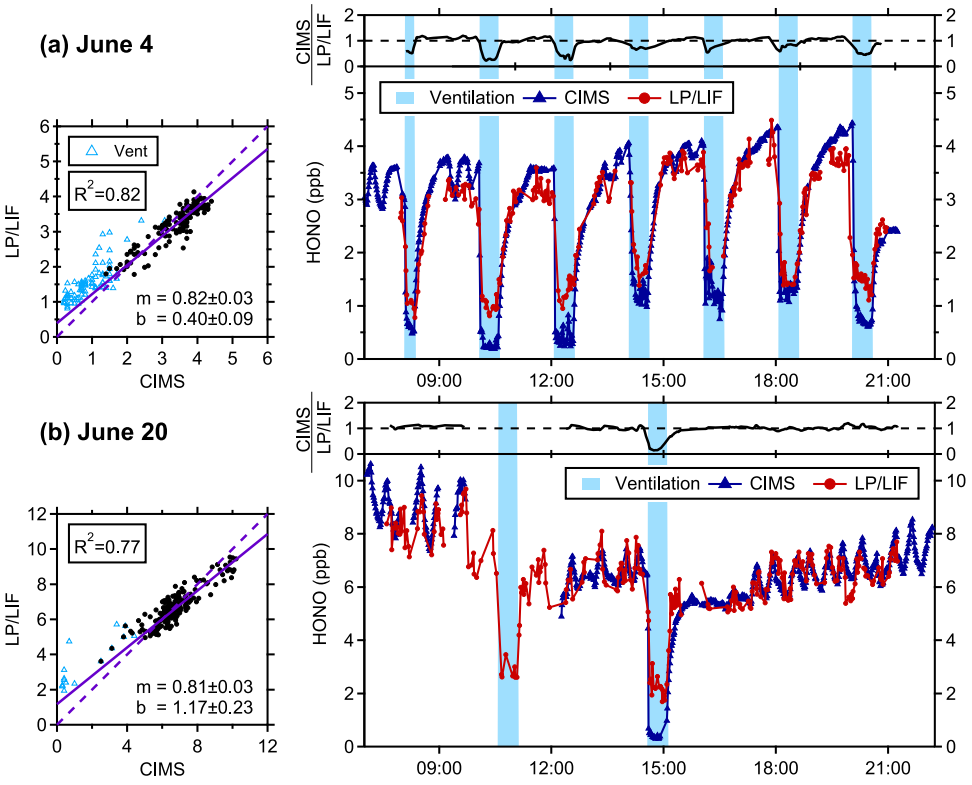

Figure 6. CIMS (blue), LP/LIF (red), and the ratio of the CIMS and LP/LIF measurements of HONO mixing during ventilation experiments (blue-shaded regions) on June 4 and 20. Measurements during ventilation periods are not included in the correlation analysis.

of surface nitrite with hypochlorous acid (HOCl) producing $ClNO_2$.[41] As this reaction removes surface nitrite, it may influence partitioning between gas-phase HONO and nitrite in surface reservoirs. HOCl likely moves from the washed surfaces through the air to partition to all other surfaces in the house, impacting the partitioning of HONO on all surfaces in the house, although additional measurements are needed to confirm this.

While observed HONO mixing ratios did eventually decrease for both instruments following each bleach cleaning event, the measurement agreement was poor immediately following the application of the bleach solution, as evident by the sudden decrease in the CIMS-to-LP/LIF ratio shown in Figure 5. On June 10, the LP/LIF instrument observed an increase in the HONO signal of nearly 3 ppb during active bleach cleaning periods. As this increase was not observed by the CIMS instrument, it is likely indicative of interference in the LP/LIF instrument. One potential interfering species is HOCl, which could photolyze at 355 nm to form OH radicals that are then excited by the 308 nm laser. Although the absorption cross section of HOCl at 355 nm is approximately 30 times lower than that of HONO,[42] HOCl mixing ratios increased to nearly 200 ppb during some bleach episodes.[41] Overall, HOCl mixing ratios and observed LP/LIF signals were only weakly correlated, but the discrepancy between the CIMS and LP/LIF measurements of HONO was greatest when HOCl exceeded 100 ppb (Figure 5a) with better agreement when HOCl mixing ratios were much lower (Figure 5b). A correlation between the HOCl mixing ratio and the difference between the LP/LIF and CIMS measurements suggests that approximately 1.5% of the HOCl was photolyzed into OH and detected as HONO, consistent with the ratio of the absorption cross sections of HONO and HOCl at the photolysis laser wavelength. A corrected LP/LIF measurement is shown in Figure 5a. Excluding the data when HOCl was likely interfering with the LP/LIF measurements, the measurements between the two instruments displayed good agreement. For the sequential chlorine mopping experiment on June 10, a weighted fit of the measurements results in a slope of 1.20 ± 0.06 and an R^2 value of 0.72. Although this interference is unlikely to be significant in most forested and urban environments where the ratio of HOCl to HONO is very low, future LP/LIF measurements will require a detailed characterization of the HOCl interference during bleach cleaning experiments, or measurements in marine environments where the expected HONO mixing ratios are only a few ppt[43] compared to HOCl mixing ratios as high as 1 ppb.[44]

Enhanced Ventilation Experiments. Experiments to enhance ventilation rates through window opening were performed to examine the dynamic equilibrium between gas-phase species and indoor surface reservoirs. During each ventilation period, all external doors and windows were fully opened for 30 min while the internal mixing rate of the house remained constant. HONO mixing ratios rapidly decreased with most ventilation periods due to mixing with outdoor air, with the ventilation period at 10:30 on June 10 (Figure 5a) an exception, and then quickly returned to high steady-state mixing ratios (3−4 ppb in Figure 6a) after the doors and windows were closed. This behavior was also observed in a similar residential setting and suggests that indoor HONO mixing ratios are strongly affected by dynamic partitioning with an interior surface reservoir in addition to emission from primary sources and formation via secondary sources.[16]

Measurements of HONO during the sequential ventilation experiment on June 4 as well as ventilation periods during a sequential natural product cleaning experiment on June 20 are

https://doi.org/10.1021/acs.est.2c02196
Environ. Sci. Technol. 2022, 56, 13573−13583

shown in Figure 6. A weighted fit of the measurements by the instruments during the June 4 sequential ventilation experiments results in a slope of 0.82 ± 0.03 and an R^2 value of 0.82. During several ventilation periods, the LP/LIF measurements of HONO did not decrease to the same extent as the CIMS measurements, despite consistent agreement during non-ventilation periods on that same day (Figure 6). Similar results were observed during the ventilation periods during the June 6 sequential cooking experiment and the June 10 sequential bleach cleaning experiment (Figures 4 and 5). The difference between the measurements during open window ventilation periods varied and is also illustrated by the CIMS-to-LP/LIF measurement ratios in Figure 6, indicating that spatial variation of HONO within the house may be significant when the windows are open. While recirculation of air may quickly distribute HONO within the closed test house, as demonstrated by agreement during cooking and cleaning events, the spatial distribution of HONO during open window ventilation periods may be influenced by external factors. In this case, the most likely explanation for the change in agreement may be that each instrument sampled a different mixture of indoor air and ambient outdoor air that moved inside as a result of changes in air circulation patterns within the house during ventilation periods. It is possible that the CIMS inlet was positioned within a cross-breeze of outdoor air moving between the open front door and kitchen window, leading to lower observed HONO concentrations compared to the LP/LIF instrument.

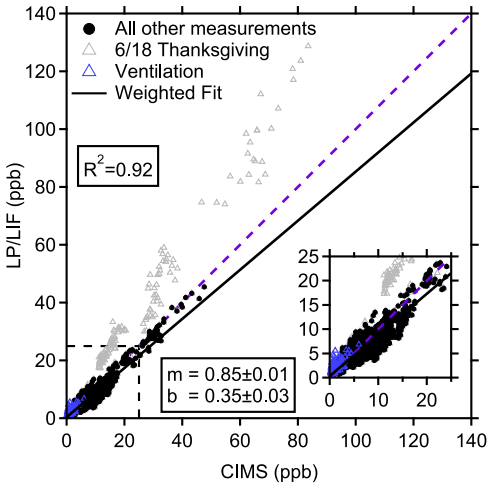

Figure 7. Correlation plot of all common measurements between the CIMS and LP/LIF instruments during HOMEChem. Gray triangles indicate measurements from the Thanksgiving experiment on June 18, during which measured mixing ratios were significantly higher than all other measurements during the campaign, and blue triangles indicate measurements during enhanced ventilation periods. These measurements, along with a small number of measurements during bleach cleaning experiments when HOCl likely interfered with the LP/LIF instrument, are not included in the correlation analysis.

DISCUSSION

Instrumental intercomparisons of indoor HONO measurements are important to validate the respective instrumental techniques and also to validate models of the spatial and temporal mixing of indoor emissions. A recent model estimates the indoor lifetime of HONO with respect to photolysis, air exchange, and deposition to be approximately 13 min, which is long enough for emissions to impact multiple rooms in a building.[45] The simultaneous measurements of HONO from the CIMS and LP/LIF instruments in different locations during HOMEChem provide important information regarding the lifetime and spatial distribution of indoor HONO emissions that can be used to validate models.

A correlation plot of all of the measurements during the campaign is shown in Figure 7. Excluding the outlier measurements of the June 18 Thanksgiving experiment, the measurements from both instruments during the campaign agreed to within their combined instrumental uncertainties. Measurements during ventilation periods and during bleach cleaning experiments are also excluded from this correlation analysis. During these periods, the sudden changes in the CIMS-to-LP/LIF ratio shown in Figures 4−6 likely indicate that the instruments sampled different air masses during ventilation periods and that an HOCl interference impacted the LP/LIF measurements during bleach cleaning events. A bivariate fit of the data weighted by the precision of both measurements resulted in a slope of 0.85 ± 0.01 and an R^2 value of 0.92 (Figure 7) with an intercept that is small relative to the range of mixing ratios observed during the campaign.[46] The overall agreement between the two instruments is quite remarkable given the different measurement techniques and gives confidence in the reliability of the calibration methods. The slope of the correlation suggests that on average the CIMS measurements were greater than LP/LIF measurements and may be indicative of a small spatial gradient between the two instruments that may or may not be significant but is consistent with the location of the CIMS instrument closer to the strong emission sources in the kitchen.

Variations in the agreement between the instruments over the course of the campaign did occur and may be related to variations associated with the LP/LIF calibration factor. While calibrations to determine the instrumental sensitivity to OH were performed regularly throughout the campaign, photolysis efficiency (PE) calibrations were limited to before and after the campaign to avoid the introduction of NO to the test house. Shifts in the alignment and overlap of the laser beams perhaps due to temperature fluctuations impacting the optical train over time likely resulted in changes in the photofragmentation efficiency and the sensitivity of the instrument to the detection of HONO. Wavelength variations may also have contributed to fluctuations in the sensitivity of the LP/LIF instrument. More frequent calibrations as well as further stabilization of the optical train will help to minimize the uncertainty associated with the sensitivity of the instrument.

While the agreement between the two instruments gives confidence in the instrumental techniques and their calibration methods, except for the June 18 Thanksgiving experiment, the strong correlation between the measurements from two different locations inside the house also provides information on the lifetime and spatial distribution of indoor HONO concentrations. Because the CIMS inlet was located in the kitchen closer to the HONO combustion source, the agreement between the two instruments suggests that the indoor lifetime of HONO was long enough for the central air handling unit to quickly distribute HONO throughout the closed house. Although mixing in the test house was faster than what can be expected in an average home due to the constantly powered HVAC fan (8 h^{-1}), this is consistent with the CFD results of Won et al.,[30] who found that HONO emissions from a fixed combustion source would be evenly distributed

https://doi.org/10.1021/acs.est.2c02196
Environ. Sci. Technol. 2022, 56, 13573−13583

throughout a simulated room with air change rates between 0.5 and 5 h^{-1}.

During HOMEChem, the kitchen area near the CIMS inlet was illuminated in the mornings through the eastern-facing windows, while the living room area near the LP/LIF detection cell was illuminated through the western-facing windows in the afternoon. On average during the campaign, the kitchen area received maximum illumination around 10:00 local time, while the living room area received maximum illumination around 17:00. The agreement in the measured HONO between the two instruments during events that occurred during different illumination periods in the morning and afternoon suggests that loss of HONO due to photolysis or photolytic production of HONO, such as from the enhanced heterogeneous reaction of surface NO_2 or grime,[31−34] may exist but are either quickly mixed indoors or are not as important relative to other sources and sinks.

Environmental Implications. The strong correlation and agreement between the HONO measurements at the two different locations in the house suggest that the indoor lifetime of HONO is long enough for it to be quickly distributed throughout a closed indoor environment depending on the internal mixing rate, confirming previous expectations.[30,45] The agreement during different illumination periods, when sunlight impacted the instrument inlets at different times during the day, also suggests that natural light levels did not significantly impact HONO mixing ratios, consistent with model predictions of the impact of sunlight on HONO levels and previous experimental studies.[19,30] In contrast, these simulations have shown that photolysis of HONO in sunlit areas can lead to significant OH radical production.[30] During afternoon cooking events when the LP/LIF detection cell was exposed to sunlight through the western-facing windows, elevated concentrations of OH from the photolysis of HONO were observed similar to those determined in previous studies[19,20] and consistent with CFD simulations.[30] Given the agreement in the measurements of HONO in the two locations, it is likely that photolysis of HONO in the kitchen area led to elevated OH concentrations when sunlight illuminated this area in the morning. A summary of OH radical production from cooking events during HOMEChem will be presented in a subsequent publication. The results of the intercomparison suggest that OH production from the photolysis of HONO could have occurred throughout the house when different areas were illuminated by sunlight at different times during the day. This suggests that the ability of HONO emissions to be quickly and evenly mixed could sustain the oxidative capacity of indoor environments.

The average outdoor air change rate of 0.5 h^{-1} during HOMEChem is typical for many residential homes.[47] Recent model simulations suggest that higher ACRs would lead to lower HONO mixing ratios but could result in higher steady-state OH concentrations in sunlit areas due to lower concentrations of radical sinks such as NO_2. However, the higher steady-state OH concentrations in the simulation did not lead to greater production of oxidation products due to the reduction in the concentration of VOCs at the higher ACR.[30] On the other hand, lower ACRs would be expected to increase HONO mixing ratios and could lead to concentration gradients in a residence due to different emission rates of HONO. Liu et al.[34] modeled the production of HONO in a 30 m^3 kitchen due to light-induced heterogeneous reactions of NO_2 with adsorbed grime. For an ACR of 0.1 h^{-1}, the modeled predicted mixing ratios of HONO under sunlit conditions were approximately 30 ppb greater than HONO production in the dark, suggesting that HONO levels could be greater in illuminated kitchen areas in an airtight residence.

The results from the enhanced ventilation experiments suggest that indoor HONO concentration gradients can occur when outdoor air moves through the house during ventilation periods. Similar to that observed previously during the SHARP campaign HONO instrument intercomparison discussed above, different sources of HONO could cause spatial differences in HONO concentrations outdoors. The results of this intercomparison suggest that indoor HONO spatial concentration gradients can be quickly dispersed when windows are closed due to rapid internal mixing and the dynamic equilibrium of HONO with surface reservoirs.[16]

The enhanced internal mixing rate used during the campaign was potentially a limitation in characterizing spatial gradients due to indoor HONO sources. Additional measurements of the spatial distribution of HONO under low ACRs and lower indoor mixing rates are needed to determine whether emissions of HONO could lead to concentration gradients inside some residences. While the instruments used in this study have the advantage of being able to measure several species simultaneously, an array of lower-cost sensors that could simultaneously measure HONO mixing ratios in several locations within a house could provide additional information regarding the spatial distribution of indoor HONO emissions.

AUTHOR INFORMATION

Corresponding Author

Brandon Bottorff − *Department of Chemistry, Indiana University, Bloomington, Indiana 47405, United States; O'Neill School of Public and Environmental Affairs, Indiana University, Bloomington, Indiana 47405, United States;* orcid.org/0000-0002-5145-0031; Email: brapbott@iu.edu

Authors

Chen Wang − *Department of Chemistry, University of Toronto, Toronto, Ontario M5S 3H6, Canada; School of Environment Science and Engineering, Southern University of Science and Technology, Shenzhen 518055, China;* orcid.org/0000-0001-9565-8777

Emily Reidy − *Department of Chemistry, Indiana University, Bloomington, Indiana 47405, United States*

Colleen Rosales − *O'Neill School of Public and Environmental Affairs, Indiana University, Bloomington, Indiana 47405, United States; Air Quality Research Center, University of California Davis, Davis, California 95616, United States;* orcid.org/0000-0002-8925-8352

Delphine K. Farmer − *Department of Chemistry, Colorado State University, Fort Collins, Colorado 80523, United States;* orcid.org/0000-0002-6470-9970

Marina E. Vance − *Department of Mechanical Engineering, University of Colorado Boulder, Boulder, Colorado 80309, United States;* orcid.org/0000-0003-0940-0353

Jonathan P. D. Abbatt − *Department of Chemistry, University of Toronto, Toronto, Ontario M5S 3H6, Canada*

Philip S. Stevens − *Department of Chemistry, Indiana University, Bloomington, Indiana 47405, United States; O'Neill School of Public and Environmental Affairs, Indiana University, Bloomington, Indiana 47405, United States;* orcid.org/0000-0001-9899-4215

https://doi.org/10.1021/acs.est.2c02196
Environ. Sci. Technol. 2022, 56, 13573−13583

Complete contact information is available at:
https://pubs.acs.org/10.1021/acs.est.2c02196

Notes

The authors declare no competing financial interest.

■ ACKNOWLEDGMENTS

This research was supported by the Alfred P. Sloan Foundation, Chemistry of Indoor Environments Program (grant nos. G-2017-9944, G-2018-11061, G-2019-11404). The authors also thank the HOMEChem science team for their collaboration throughout the campaign.

■ REFERENCES

(1) Rohrer, F.; Berresheim, H. Strong correlation between levels of tropospheric hydroxyl radicals and solar ultraviolet radiation. *Nature* **2006**, *442*, 184−187.

(2) Tan, D.; Faloona, I.; Simpas, J. B.; Brune, W.; Shepson, P. B.; Couch, T. L.; Sumner, A. L.; Carroll, M. A.; Thornberry, T.; Apel, E.; Riemer, D.; Stockwell, W. HO_x budgets in a deciduous forest: Results from the PROPHET summer 1998 campaign. *J. Geophys. Res.: Atmos.* **2001**, *106*, 24407−24427.

(3) Griffith, S. M.; Hansen, R. F.; Dusanter, S.; Michoud, V.; Gilman, J. B.; Kuster, W. C.; Veres, P. R.; Graus, M.; de Gouw, J. A.; Roberts, J.; Young, C.; Washenfelder, R.; Brown, S. S.; Thalman, R.; Waxman, E.; Volkamer, R.; Tsai, C.; Stutz, J.; Flynn, J. H.; Grossberg, N.; Lefer, B.; Alvarez, S. L.; Rappenglueck, B.; Mielke, L. H.; Osthoff, H. D.; Stevens, P. S. Measurements of hydroxyl and hydroperoxy radicals during CalNex-LA: Model comparisons and radical budgets. *J. Geophys. Res.: Atmos.* **2016**, *121*, 4211−4232.

(4) Kleffmann, J.; Gavriloaiei, T.; Hofzumahaus, A.; Holland, F.; Koppmann, R.; Rupp, L.; Schlosser, E.; Siese, M.; Wahner, A. Daytime formation of nitrous acid: A major source of OH radicals in a forest *Geophys. Res. Lett.* 2005, *32*, L05818 DOI: 10.1029/2005GL022524.

(5) Acker, K.; Möller, D.; Wieprecht, W.; Meixner, F. X.; Bohn, B.; Gilge, S.; Plass-Dülmer, C.; Berresheim, H. Strong daytime production of OH from HNO_2 at a rural mountain site *Geophys. Res. Lett.* 2006, *332*, L02809 DOI: 10.1029/2005gl024643.

(6) Ren, X.; van Duin, D.; Cazorla, M.; Chen, S.; Mao, J.; Zhang, L.; Brune, W. H.; Flynn, J. H.; Grossberg, N.; Lefer, B. L.; Rappenglück, B.; Wong, K. W.; Tsai, C.; Stutz, J.; Dibb, J. E.; Thomas Jobson, B.; Luke, W. T.; Kelley, P. Atmospheric oxidation chemistry and ozone production: Results from SHARP 2009 in Houston, Texas. *J. Geophys. Res.: Atmos.* **2013**, *118*, 5770−5780.

(7) Slater, E. J.; Whalley, L. K.; Woodward-Massey, R.; Ye, C.; Lee, J. D.; Squires, F.; Hopkins, J. R.; Dunmore, R. E.; Shaw, M.; Hamilton, J. F.; Lewis, A. C.; Crilley, L. R.; Kramer, L.; Bloss, W.; Vu, T.; Sun, Y.; Xu, W.; Yue, S.; Ren, L.; Acton, W. J. F.; Hewitt, C. N.; Wang, X.; Fu, P.; Heard, D. E. Elevated levels of OH observed in haze events during wintertime in central Beijing. *Atmos. Chem. Phys.* **2020**, *20*, 14847−14871.

(8) Kim, S.; VandenBoer, T. C.; Young, C. J.; Riedel, T. P.; Thornton, J. A.; Swarthout, B.; Sive, B.; Lerner, B.; Gilman, J. B.; Warneke, C.; Roberts, J. M.; Guenther, A.; Wagner, N. L.; Dubé, W. P.; Williams, E.; Brown, S. S. The primary and recycling sources of OH during the NACHTT-2011 campaign: HONO as an important OH primary source in the wintertime. *J. Geophys. Res.: Atmos.* **2014**, *119*, 6886−6896.

(9) Ma, X.; Tan, Z.; Lu, K.; Yang, X.; Liu, Y.; Li, S.; Li, X.; Chen, S.; Novelli, A.; Cho, C.; Zeng, L.; Wahner, A.; Zhang, Y. Winter photochemistry in Beijing: Observation and model simulation of OH and HO2 radicals at an urban site. *Sci. Total Environ.* **2019**, *685*, 85−95.

(10) Lee, K.; Xue, J.; Geyh, A. S.; Ozkaynak, H.; Leaderer, B. P.; Weschler, C. J.; Spengler, J. D. Nitrous acid, nitrogen dioxide, and ozone concentrations in residential environments. *Environ. Health Perspect.* **2002**, *110*, 145−149.

(11) Leaderer, B. P.; Naeher, L.; Jankun, T.; Balenger, K.; Holford, T. R.; Toth, C.; Sullivan, J.; Wolfson, J. M.; Koutrakis, P. Indoor, outdoor, and regional summer and winter concentrations of PM_{10}, $PM_{2.5}$, SO_4^{2-}, H^+, NH_4^+, NO_3^-, NH_3, and nitrous acid in homes with and without kerosene space heaters. *Environ. Health Perspect.* **1999**, *107*, 223−231.

(12) Liu, J.; Li, S.; Zeng, J.; Mekic, M.; Yu, Z.; Zhou, W.; Loisel, G.; Gandolfo, A.; Song, W.; Wang, X.; Zhou, Z.; Herrmann, H.; Li, X.; Gligorovski, S. Assessing indoor gas phase oxidation capacity through real-time measurements of HONO and NOx in Guangzhou, China. *Environ. Sci.: Processes Impacts* **2019**, *21*, 1393−1402.

(13) Zhou, S.; Young, C. J.; VandenBoer, T. C.; Kowal, S. F.; Kahan, T. F. Time-Resolved Measurements of Nitric Oxide, Nitrogen Dioxide, and Nitrous Acid in an Occupied New York Home. *Environ. Sci. Technol.* **2018**, *52*, 8355−8364.

(14) Brauer, M.; Ryan, P. B.; Suh, H. H.; Koutrakis, P.; Spengler, J. D.; Leslie, N. P.; Billick, I. H. Measurements of nitrous acid inside two research houses. *Environ. Sci. Technol.* **1990**, *24*, 1521−1527.

(15) Vecera, Z.; Dasgupta, P. K. Indoor Nitrous Acid Levels. Production of Nitrous Acid from Open-Flame Sources. *Int. J. Environ. Anal. Chem.* **1994**, *56*, 311−316.

(16) Collins, D. B.; Hems, R. F.; Zhou, S.; Wang, C.; Grignon, E.; Alavy, M.; Siegel, J. A.; Abbatt, J. P. D. Evidence for Gas−Surface Equilibrium Control of Indoor Nitrous Acid. *Environ. Sci. Technol.* **2018**, *52*, 12419−12427.

(17) Wang, C.; Collins, D. B.; Arata, C.; Goldstein, A. H.; Mattila, J. M.; Farmer, D. K.; Ampollini, L.; DeCarlo, P. F.; Novoselac, A.; Vance, M. E.; Nazaroff, W. W.; Abbatt, J. P. D. Surface reservoirs dominate dynamic gas-surface partitioning of many indoor air constituents. *Sci. Adv.* **2020**, *6*, No. eaay8973.

(18) Wang, C.; Bottorff, B.; Reidy, E.; Rosales, C. M. F.; Collins, D. B.; Novoselac, A.; Farmer, D. K.; Vance, M. E.; Stevens, P. S.; Abbatt, J. P. D. Cooking, Bleach Cleaning, and Air Conditioning Strongly Impact Levels of HONO in a House. *Environ. Sci. Technol.* **2020**, *54*, 13488−13497.

(19) Gómez Alvarez, E.; Amedro, D.; Afif, C.; Gligorovski, S.; Schoemaecker, C.; Fittschen, C.; Doussin, J.-F.; Wortham, H. Unexpectedly high indoor hydroxyl radical concentrations associated with nitrous acid. *Proc. Natl. Acad. Sci. U.S.A.* **2013**, *110*, 13294−13299.

(20) Bartolomei, V.; Gómez Alvarez, E.; Wittmer, J.; Tlili, S.; Strekowski, R.; Temime-Roussel, B.; Quivet, E.; Wortham, H.; Zetzsch, C.; Kleffmann, J.; Gligorovski, S. Combustion Processes as a Source of High Levels of Indoor Hydroxyl Radicals through the Photolysis of Nitrous Acid. *Environ. Sci. Technol.* **2015**, *49*, 6599−6607.

(21) Kowal, S. F.; Allen, S. R.; Kahan, T. F. Wavelength-Resolved Photon Fluxes of Indoor Light Sources: Implications for HO_x Production. *Environ. Sci. Technol.* **2017**, *51*, 10423−10430.

(22) Spataro, F.; Ianniello, A. Sources of atmospheric nitrous acid: State of the science, current research needs, and future prospects. *J. Air Waste Manage. Assoc.* **2014**, *64*, 1232−1250.

(23) Kleffmann, J.; Lörzer, J. C.; Wiesen, P.; Kern, C.; Trick, S.; Volkamer, R.; Rodenas, M.; Wirtz, K. Intercomparison of the DOAS and LOPAP techniques for the detection of nitrous acid (HONO). *Atmos. Environ.* **2006**, *40*, 3640−3652.

(24) Kleffmann, J.; Wiesen, P. Technical Note: Quantification of interferences of wet chemical HONO LOPAP measurements under simulated polar conditions. *Atmos. Chem. Phys.* **2008**, *8*, 6813−6822.

(25) Heland, J.; Kleffmann, J.; Kurtenbach, R.; Wiesen, P. A New Instrument To Measure Gaseous Nitrous Acid (HONO) in the Atmosphere. *Environ. Sci. Technol.* **2001**, *35*, 3207−3212.

(26) Stutz, J.; Oh, H.-J.; Whitlow, S. I.; Anderson, C.; Dibb, J. E.; Flynn, J. H.; Rappenglück, B.; Lefer, B. Simultaneous DOAS and mist-chamber IC measurements of HONO in Houston, TX. *Atmos. Environ.* **2010**, *44*, 4090−4098.

(27) Ródenas, M.; Muñoz, A.; Alacreu, F.; Brauers, T.; Dorn, H.-P.; Kleffmann, J.; Bloss, W. Assessment of HONO Measurements: The FIONA Campaign at EUPHORE. In *Disposal of Dangerous Chemicals in Urban Areas and Mega Cities*,Barnes, I.; Rudziński, K. J., Eds.; Springer Netherlands: Dordrecht, 2013; pp 45−58.
(28) Pinto, J. P.; Dibb, J.; Lee, B. H.; Rappenglück, B.; Wood, E. C.; Levy, M.; Zhang, R.-Y.; Lefer, B.; Ren, X.-R.; Stutz, J.; Tsai, C.; Ackermann, L.; Golovko, J.; Herndon, S. C.; Oakes, M.; Meng, Q.-Y.; Munger, J. W.; Zahniser, M.; Zheng, J. Intercomparison of field measurements of nitrous acid (HONO) during the SHARP campaign. *J. Geophys. Res.: Atmos.* **2014**, *119*, 5583−5601.
(29) Crilley, L. R.; Kramer, L. J.; Ouyang, B.; Duan, J.; Zhang, W.; Tong, S.; Ge, M.; Tang, K.; Qin, M.; Xie, P.; Shaw, M. D.; Lewis, A. C.; Mehra, A.; Bannan, T. J.; Worrall, S. D.; Priestley, M.; Bacak, A.; Coe, H.; Allan, J.; Percival, C. J.; Popoola, O. A. M.; Jones, R. L.; Bloss, W. J. Intercomparison of nitrous acid (HONO) measurement techniques in a megacity (Beijing). *Atmos. Meas. Tech.* **2019**, *12*, 6449−6463.
(30) Won, Y.; Waring, M.; Rim, D. Understanding the Spatial Heterogeneity of Indoor OH and HO2 due to Photolysis of HONO Using Computational Fluid Dynamics Simulation. *Environ. Sci. Technol.* **2019**, *53*, 14470−14478.
(31) Bartolomei, V.; Sörgel, M.; Gligorovski, S.; Gómez Alvarez, E.; Gandolfo, A.; Strekowski, R.; Quivet, E.; Held, A.; Zetzsch, C.; Wortham, H. Formation of indoor nitrous acid (HONO) by light-induced NO_2 heterogeneous reactions with white wall paint. *Environ. Sci. Pollut. Res.* **2014**, *21*, 9259−9269.
(32) Gómez Alvarez, E.; Sörgel, M.; Gligorovski, S.; Bassil, S.; Bartolomei, V.; Coulomb, B.; Zetzsch, C.; Wortham, H. Light-induced nitrous acid (HONO) production from NO_2 heterogeneous reactions on household chemicals. *Atmos. Environ.* **2014**, *95*, 391−399.
(33) Gandolfo, A.; Bartolomei, V.; Gómez Alvarez, E.; Tlili, S.; Gligorovski, S.; Kleffmann, J.; Wortham, H. The effectiveness of indoor photocatalytic paints on NO_x and HONO levels. *Appl. Catal., B* **2015**, *166−167*, 84−90.
(34) Liu, J.; Deng, H.; Lakey, P. S. J.; Jiang, H.; Mekic, M.; Wang, X.; Shiraiwa, M.; Gligorovski, S. Unexpectedly High Indoor HONO Concentrations Associated with Photochemical NO_2 Transformation on Glass Windows. *Environ. Sci. Technol.* **2020**, *54*, 15680−15688.
(35) Farmer, D. K.; Vance, M. E.; Abbatt, J. P. D.; Abeleira, A.; Alves, M. R.; Arata, C.; Boedicker, E.; Bourne, S.; Cardoso-Saldaña, F.; Corsi, R.; DeCarlo, P. F.; Goldstein, A. H.; Grassian, V. H.; Hildebrandt Ruiz, L.; Jimenez, J. L.; Kahan, T. F.; Katz, E. F.; Mattila, J. M.; Nazaroff, W. W.; Novoselac, A.; O'Brien, R. E.; Or, V. W.; Patel, S.; Sankhyan, S.; Stevens, P. S.; Tian, Y.; Wade, M.; Wang, C.; Zhou, S.; Zhou, Y. Overview of HOMEChem: House Observations of Microbial and Environmental Chemistry. *Environ. Sci.: Processes Impacts* **2019**, *21*, 1280−1300.
(36) Bottorff, B.; Reidy, E.; Mielke, L.; Dusanter, S.; Stevens, P. S. Development of a laser-photofragmentation laser-induced fluorescence instrument for the detection of nitrous acid and hydroxyl radicals in the atmosphere. *Atmos. Meas. Tech.* **2021**, *14*, 6039−6056.
(37) Dusanter, S.; Vimal, D.; Stevens, P. S. Technical note: Measuring tropospheric OH and HO_2 by laser-induced fluorescence at low pressure. A comparison of calibration techniques. *Atmos. Chem. Phys.* **2008**, *8*, 321−340.
(38) Dusanter, S.; Vimal, D.; Stevens, P. S.; Volkamer, R.; Molina, L. T. Measurements of OH and HO_2 concentrations during the MCMA-2006 field campaign − Part 1: Deployment of the Indiana University laser-induced fluorescence instrument. *Atmos. Chem. Phys.* **2009**, *9*, 1665−1685.
(39) Roberts, J. M.; Veres, P.; Warneke, C.; Neuman, J. A.; Washenfelder, R. A.; Brown, S. S.; Baasandorj, M.; Burkholder, J. B.; Burling, I. R.; Johnson, T. J.; Yokelson, R. J.; de Gouw, J. Measurement of HONO, HNCO, and other inorganic acids by negative-ion proton-transfer chemical-ionization mass spectrometry (NI-PT-CIMS): application to biomass burning emissions. *Atmos. Meas. Tech.* **2010**, *3*, 981−990.
(40) Wong, J. P. S.; Carslaw, N.; Zhao, R.; Zhou, S.; Abbatt, J. P. D. Observations and impacts of bleach washing on indoor chlorine chemistry. *Indoor Air* **2017**, *27*, 1082−1090.
(41) Mattila, J. M.; Lakey, P. S. J.; Shiraiwa, M.; Wang, C.; Abbatt, J. P. D.; Arata, C.; Goldstein, A. H.; Ampollini, L.; Katz, E. F.; DeCarlo, P. F.; Zhou, S.; Kahan, T. F.; Cardoso-Saldaña, F. J.; Ruiz, L. H.; Abeleira, A.; Boedicker, E. K.; Vance, M. E.; Farmer, D. K. Multiphase Chemistry Controls Inorganic Chlorinated and Nitrogenated Compounds in Indoor Air during Bleach Cleaning. *Environ. Sci. Technol.* **2020**, *54*, 1730−1739.
(42) Burkholder, J. B.; Sander, S. P.; Abbatt, J.; Barker, J. R.; Cappa, C.; Crounse, J. D.; Dibble, T. S.; Huie, R. E.; Kolb, C. E.; Kurylo, M. J.; Orkin, V. L.; Percival, C. J.; Wilmouth, D. M.; Wine, P. H. *Chemical Kinetics and Photochemical Data for Use in Atmospheric Studies, Evaluation No. 19*; JPL Publication: 19-5, Jet Propulsion Laboratory, Pasadena, 2020.
(43) Crilley, L. R.; Kramer, L. J.; Pope, F. D.; Reed, C.; Lee, J. D.; Carpenter, L. J.; Hollis, L. D. J.; Ball, S. M.; Bloss, W. J. Is the ocean surface a source of nitrous acid (HONO) in the marine boundary layer? *Atmos. Chem. Phys.* **2021**, *21*, 18213−18225.
(44) Lawler, M. J.; Sander, R.; Carpenter, L. J.; Lee, J. D.; von Glasow, R.; Sommariva, R.; Saltzman, E. S. HOCl and Cl_2 observations in marine air. *Atmos. Chem. Phys.* **2011**, *11*, 7617−7628.
(45) Lakey, P. S. J.; Won, Y.; Shaw, D.; Østerstrøm, F. F.; Mattila, J.; Reidy, E.; Bottorff, B.; Rosales, C.; Wang, C.; Ampollini, L.; Zhou, S.; Novoselac, A.; Kahan, T. F.; DeCarlo, P. F.; Abbatt, J. P. D.; Stevens, P. S.; Farmer, D. K.; Carslaw, N.; Rim, D.; Shiraiwa, M. Spatial and temporal scales of variability for indoor air constituents. *Commun. Chem.* **2021**, *4*, No. 110.
(46) Cantrell, C. A. Technical Note: Review of methods for linear least-squares fitting of data and application to atmospheric chemistry problems. *Atmos. Chem. Phys.* **2008**, *8*, 5477−5487.
(47) Murray, D. M.; Burmaster, D. E. Residential Air Exchange Rates in the United States: Empirical and Estimated Parametric Distributions by Season and Climatic Region. *Risk Anal.* **1995**, *15*, 459−465.

https://doi.org/10.1021/acs.est.2c02196
Environ. Sci. Technol. 2022, 56, 13573−13583